Orbital ice: An exact Coulomb phase on the diamond lattice

Gia-Wei Chern[1] and Congjun Wu[2]
[1]*Department of Physics, University of Wisconsin, Madison, Wisconsin 53706, USA*
[2]*Department of Physics, University of California, San Diego, California 92093, USA*
(Received 13 April 2011; revised manuscript received 26 November 2011; published 15 December 2011)

We demonstrate the existence of an orbital Coulomb phase as the exact ground state of a p-orbital exchange Hamiltonian on the diamond lattice. The Coulomb phase is an emergent state characterized by algebraic dipolar correlations and a gauge structure resulting from local constraints (ice rules) of the underlying lattice models. For most ice models on the pyrochlore lattice, these local constraints are a direct consequence of minimizing the energy of each individual tetrahedron. On the contrary, the orbital ice rules are emergent phenomena resulting from the quantum orbital dynamics. We show that the orbital ice model exhibits an emergent geometrical frustration by mapping the degenerate quantum orbital ground states to the spin-ice states obeying the 2-in-2-out constraints on the pyrochlore lattice. We also discuss possible realization of the orbital ice model in optical lattices with p-band fermionic cold atoms.

DOI: 10.1103/PhysRevE.84.061127 PACS number(s): 05.50.+q, 03.75.Ss, 71.10.Fd, 73.43.Nq

I. INTRODUCTION

Common water ice, a strongly correlated proton system, is a canonical example of geometrical frustration [1]. The oxygen ions in ice form a periodic diamond lattice whereas the protons are disordered due to the frustrated arrangement of two inequivalent O–H bonds with different lengths. This in turn leads to a macroscopic degeneracy of possible ground states and a finite entropy density of ice as temperature tends toward zero. Despite being disordered, the positioning of protons dictated by the so-called ice rules exhibits a strong short-range correlation in which each oxygen ion has two-near and two-far protons. The ice rules also forbid single-proton hopping and only allow ring-exchange-type motion, reminiscent of the physics of gauge theory.

A magnetic analog of ice was discovered in the pyrochlore oxides $Dy_2Ti_2O_7$ and $Ho_2Ti_2O_7$ more than a decade ago [2]. These so-called spin-ice compounds are essentially pyrochlore Ising magnets in which magnetic moments residing on a network of corner-sharing tetrahedra are forced by single-ion anisotropy to point along the local $\langle 111\rangle$ axes. It is found that extensively degenerate spin configurations obeying the so-called 2-in-2-out rules have essentially the same energy over a wide range of temperatures. The measured residual entropy is well approximated by the Pauling entropy for water ice [3]. These local constraints require that every tetrahedron has two spins pointing in and two pointing out, in apparent analogy with the ice rules. Reversing a single spin in the ice state creates one defect tetrahedron with 3-in-1-out spins and another one with 1-in-3-out spins. As recently pointed out in Ref. [4], these defect tetrahedra behave exactly as a gas of magnetic monopoles interacting with each other via Coulomb's $1/r$ law.

Artificial versions of spin ice have also been created using lithographically fabricated arrays of nanoscale magnets [5,6]. Other proposals of artificial ice systems include charged colloidals in optical traps and superconducting vortices in specially fabricated pinning centers [7,8]. A valence bond liquid phase with an ice-like degeneracy is also shown to be the ground state of a spin-1/2 Klein model on the pyrochlore lattice [9].

In most of these ice systems, the fundamental degrees of freedom are doublet variables defined on the pyrochlore lattice or its two-dimensional counterpart. Their Hamiltonians can often be cast into the form

$$H_{\rm ice} = J\sum_{\boxtimes}\mathcal{K}_{\boxtimes} + \epsilon\, H', \tag{1}$$

where $J>0$ is the energy scale of excitations and the sum is over all tetrahedra. $\mathcal{K}_{\boxtimes}$ is a non-negative-definite operator defined for a tetrahedron. The last term denotes perturbations of energy scale ϵ. The ice rules correspond to the constraints

$$\mathcal{K}_{\boxtimes} = 0 \tag{2}$$

for all tetrahedra. Taking spin ice as an example, the spin configurations can be specified by a set of Ising variables $\{\sigma_i\}$ such that $\mathbf{S}_i = \sigma_i S\,\hat{\mathbf{e}}_i$, where $\hat{\mathbf{e}}_i$ denotes the local easy axis. The constraint operator is then given by $\mathcal{K}_{\boxtimes}\propto(Q_{\boxtimes})^2$, where $Q_{\boxtimes}\equiv\sum_{m\in\boxtimes}\sigma_m$ is the effective magnetic charge of a tetrahedron. The six up-up-down-down Ising configurations selected by constraints (2) correspond to the 2-in-2-out rules. Another example is the spin-1/2 Klein model for which $\mathcal{K}_{\boxtimes}\equiv\mathcal{P}_{S_{\boxtimes}=2}$ is the projection operator onto the subspace of maximum total spin $S_{\boxtimes}=2$ [9]. For temperatures in the regime $\epsilon\ll T\ll J$, configurations satisfying the "ice rules" (2) for all tetrahedra, are effectively degenerate.

The ice model (1) hosts an emergent Coulomb phase in which the local constraints $\mathcal{K}_{\boxtimes}=0$ translate to a divergence-free flux $\nabla\cdot\mathbf{B}=0$ in the coarse-grained approximation. The effective theory for the Coulomb phase is equivalent to conventional magnetostatics [10]. It follows that both the "magnetic" field $\mathbf{B}$ and spins $\mathbf{S}_i$ in this disordered yet highly constrained phase exhibit a dipolar-like correlation function $\langle B_\alpha(0)B_\beta(\mathbf{r})\rangle\propto(\delta_{\alpha\beta}-3\hat{r}_\alpha\hat{r}_\beta)/r^3$ at large distances.

In this paper, we present an ice model in which the basic degrees of freedom are triplet orbital variables defined on the *diamond* lattice. Our investigation is partly motivated by recent progress in orbital-related many-body phenomena in optical lattices. We show that the strong directional dependence of orbital exchange combined with the special geometry of diamond lattices gives rise to a huge degeneracy in the

Gutzwiller-type ground states which are also exact eigenstates of the orbital exchange Hamiltonian. We demonstrate the existence of an orbital Coulomb phase by mapping the degenerate orbital manifold to spin-ice states on the medial pyrochlore lattice. It is worth noting that the orbital "ice rules" are *not* constraints imposed by the Hamiltonian. Instead, they are emergent properties characterizing the short-range orbital correlations. This is in stark contrast to the pyrochlore ice models of Eq. (1) in which the ice rules are explicitly incorporated in the Hamiltonian as the minimum energy states of the individual tetrahedron.

II. ORBITAL EXCHANGE HAMILTONIAN

The ability to precisely control the interaction strength of cold atoms in optical lattices provides clean realizations of strongly correlated models without the many undesirable complexities usually encountered in material systems [11,12]. In particular, since the cold-atom systems are free of Jahn-Teller distortions, they offer a new opportunity to investigate the intrinsic exchange physics associated with the orbital degrees of freedom [13]. One of the most interesting directions is the novel frustration phenomenon originating from the anisotropic orbital interactions.

The exchange physics of p orbitals in two-dimensional optical lattices has been extensively discussed in Refs. [14,15]. The intricate interplay between lattice geometry and anisotropic orbital exchange leads to dramatically distinct ground states in different lattices. The orbital exchange on a square lattice is dominated by an antiferromagnetic Ising-like Hamiltonian, which gives rise to a Néel-type orbital order. For triangular, honeycomb, and kagome lattices, the orbital interaction is described by a novel quantum 120° model. Although long-range orbital orders occur in the cases of triangular and kagome lattices, orbital interactions are frustrated on the bipartite honeycomb lattice and a huge degeneracy remains in the classical ground state. These highly degenerate ground states can be mapped to fully packed non-intersecting loops on the honeycomb lattice. Quantum fluctuations, on the other hand, select a six-site plaquette ground state through order from disorder mechanism. The 120° model also describes the effective orbital interaction in transition metal oxides including honeycomb, cubic, and pyrochlore lattices [16–18].

Here we consider a p-band Hubbard model with spinless fermions on three-dimensional optical lattices. We assume that each optical site is approximated by an isotropic harmonic potential. For two particles per site, one of them fills the inert s orbital while the other one occupies one of the three p orbitals. The kinetic terms of p-band fermions include a longitudinal $t_\parallel$ and a transverse $t_\perp$ hopping, corresponding to σ and π bondings, respectively. Typically, $t_\parallel \gg t_\perp$ [19] and we shall neglect the transverse hopping as a zeroth-order approximation. The fermions interact with each other through an on-site repulsion: $H_{\rm int} = U \sum_{i,\alpha\neq\beta} n_{i\alpha} n_{i\beta}$, where $n_{i\alpha} = p^\dagger_{i\alpha} p_{i\alpha}$ is the fermion number operator. The leading contribution to U comes from the p-wave scattering for spinless fermions. The strong correlation regime $U \gg t_\parallel$ can be potentially realized with the aid of the recently proposed stable optical p-wave Feshbach resonance [20], which has the advantage of suppressing the high rate of three-body recombination. It should be noted that recent experimental results have shown some limitations of the optical s-wave Feshbach scheme [21]. Further experimental investigations are needed to verify the feasibility of increasing p-wave interaction through optical Feshbach resonance.

With charge fluctuations suppressed in the Mott-insulating limit, there still remains a triplet orbital degrees of freedom at each site. Exchange interactions between these localized orbital variables originate from the second-order virtual hopping of the fermions. Since we assume a dominating $t_\parallel$, for a bond parallel to $\hat{\mathbf{n}} = (n_x, n_y, n_z)$, longitudinal hopping is possible only when one of the particles occupies the orbital $|\hat{\mathbf{n}}\rangle = n_x|p_x\rangle + n_y|p_y\rangle + n_z|p_z\rangle$, while the other one is in an orthogonal state. The energy gain of such an antiferro-orbital alignment is described by the Hamiltonian

$$H_{\rm ex} = -J \sum_{\langle ij\rangle} \left[P_i^{\hat{\mathbf{n}}_{ij}} \left(I - P_j^{\hat{\mathbf{n}}_{ij}}\right) + \left(I - P_i^{\hat{\mathbf{n}}_{ij}}\right) P_j^{\hat{\mathbf{n}}_{ij}} \right]. \quad (3)$$

Here $J = t_\parallel^2/U$ sets the exchange energy scale, I is the identity operator, and $P^{\hat{\mathbf{n}}_{ij}} = |\hat{\mathbf{n}}_{ij}\rangle\langle\hat{\mathbf{n}}_{ij}|$ is the projection operator of the active orbital on a nearest-neighbor bond $\langle ij\rangle$. Obviously, the nature of the orbital exchange physics depends critically on the lattice geometry.

III. CUBIC OPTICAL LATTICE

As a warm-up, we first consider the case of a cubic lattice [Fig. 1(a)]. Using a basis spanned by $|p_x\rangle$, $|p_y\rangle$, and $|p_z\rangle$ states, the orbital projectors along the x, y, and z bonds can be expressed in terms of Gell-Mann matrices $\lambda^{(3)} = \mathrm{diag}(1,-1,0)$ and $\lambda^{(8)} = \mathrm{diag}(1,1,-2)/\sqrt{3}$. By grouping them into a doublet operator $\boldsymbol{\tau} = (\tau^x, \tau^y) = (\sqrt{3}/2)(\lambda^{(8)}, \lambda^{(3)})$, the three orbital projectors are

$$P^a = (I + 2\,\boldsymbol{\tau}\cdot\hat{\mathbf{e}}_a)/3, \quad (a = x,y,z), \quad (4)$$

with $\hat{\mathbf{e}}_{x/y} = (\pm\frac{\sqrt{3}}{2}, \frac{1}{2})$ and $\hat{\mathbf{e}}_z = (0,-1)$ [Fig. 1(a)]. The expectation value of the doublet vector $\langle\boldsymbol{\tau}\rangle$ represents the disparities of on-site orbital occupation numbers. The domain of $\langle\boldsymbol{\tau}\rangle$ is an equilateral triangle [Fig. 1(b)], whose three corners, $\langle\boldsymbol{\tau}\rangle = \hat{\mathbf{e}}_x, \hat{\mathbf{e}}_y$, and $\hat{\mathbf{e}}_z$, correspond to states with pure p_x, p_y, and p_z orbitals, respectively. Substituting the projectors P^a into Eq. (3), we obtain an effective Hamiltonian

$$H_{\rm cubic} = \frac{8J}{9} \sum_{a=x,y,z} \sum_{\langle ij\rangle\parallel a} (\boldsymbol{\tau}_i\cdot\hat{\mathbf{e}}_a)(\boldsymbol{\tau}_j\cdot\hat{\mathbf{e}}_a), \quad (5)$$

up to an irrelevant constant $c_0 = -4NJ/3$. Although Eq. (5) has the same form as the well-known 120° model, it is actually a classical Hamiltonian since the three orbital projectors P^a commute with each other. As a result, the eigenstates of $H_{\rm cubic}$ are simultaneous eigenstates of the orbital occupation operators P_i^a whose eigenvalues are 0 or 1. Since each site has exactly one fermion, $P^x + P^y + P^z = 1$, the orbital state at a given site can be specified by one of the three corners in the triangular domain of $\langle\boldsymbol{\tau}\rangle$. Equation (5) can then be viewed as a three-state Potts model with anisotropic interactions. An x bond, for example, has three different orbital configurations, (p_x, p_x), $(p_{y/z}, p_{y/z})$, and $(p_x, p_{y/z})$, whose energies are $8J/9$, $2J/9$, and $-4J/9$, respectively.

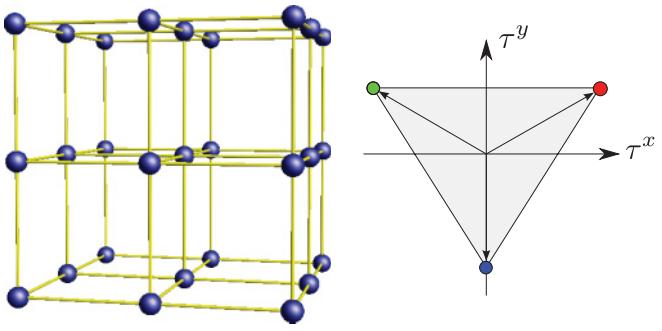

FIG. 1. (Color online) (a) Cubic optical lattice. (b) Domain of doublet vector $\langle \boldsymbol{\tau} \rangle$ for the cubic lattice. Beginning with the upper right corner, the three corners correspond to p_x, p_y, and p_z orbitals, respectively.

To investigate the orbital correlations in the ground state, we performed classical Monte Carlo simulations with periodic boundary conditions on systems up to $N = 24^3$ sites. Figures 2(a) and 2(b) show the average bond energy ϵ, specific heat c, and entropy density s as functions of temperature T. The bond energy approaches $\epsilon_0 = -2J/9$ as $T \to 0$, implying that 2/3 of the bonds with an energy $\epsilon = -4J/9$ are in the antiferro-orbital ground states, while the remaining 1/3 are frustrated with an energy of $2J/9$. The macroscopic degeneracy of the ground states is evidenced by a residual entropy density $s_0 \approx 0.599\, k_B$ obtained by integrating the specific-heat curve [Fig. 2(b)]. The orbital correlation $C_\tau(r) = \langle \boldsymbol{\tau}(r) \cdot \boldsymbol{\tau}(0) \rangle$ decays rather fast and is negligible beyond $r \approx 5$, indicating a disordered orbital liquid. At large separations, the correlation function decays exponentially as shown in Fig. 2(c).

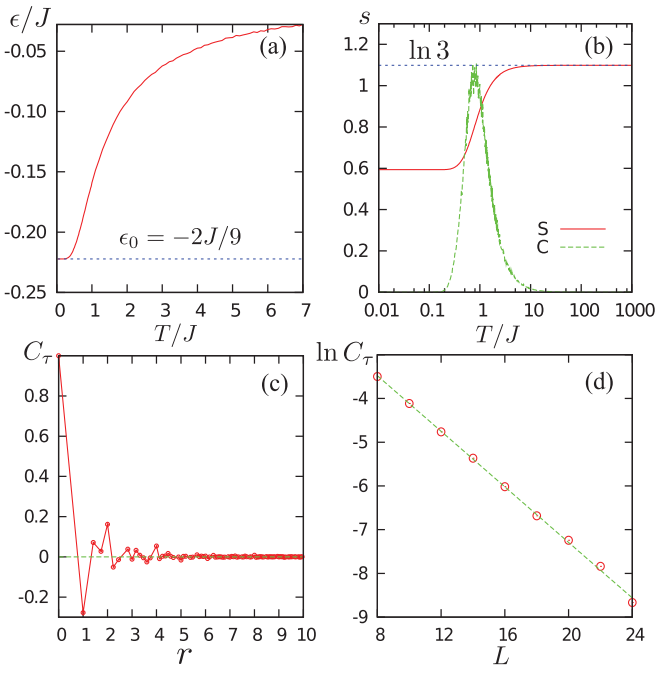

FIG. 2. (Color online) Monte Carlo simulations of the classical Hamiltonian (5). (a) Temperature dependence of average bond energy $\epsilon \equiv \langle H_{\text{cubic}} \rangle / 3N$. (b) Specific heat c and entropy density s. The dashed line in (b) indicates the entropy density $\ln 3$ at the high-temperature para-orbital phase. (c) Orbital correlation function $C_\tau(r) = \langle \boldsymbol{\tau}(r) \cdot \boldsymbol{\tau}(0) \rangle$ as a function of separation r. (d) $\ln C_\tau(L/2)$ as a function of linear system size L.

The large residual entropy $s_0 \approx 0.599\, k_B$ also implies that the ground state is susceptible to nominally small perturbations present in the system. Indeed, as recently reported in Ref. [22], inclusion of orbital interactions which break time-reversal symmetry induces long-range orbital ordering. As a final remark, it is worth noting that Eq. (5) is related to but quite different from the 120° model with classical O(2) spins, in which orbital-ordering is shown to be induced via an order-from-disorder mechanism on the cubic lattice [23–25].

IV. DIAMOND OPTICAL LATTICE

We now turn to orbital exchange on the oblique diamond lattice [Fig. 3(a)]. There are four distinct types of nearest-neighbor bonds pointing along directions $\hat{\mathbf{n}}_0 = [111]$, $\hat{\mathbf{n}}_1 = [1\bar{1}\bar{1}]$, $\hat{\mathbf{n}}_2 = [\bar{1}1\bar{1}]$, and $\hat{\mathbf{n}}_3 = [\bar{1}\bar{1}1]$. Experimentally, a diamond optical lattice can be generated by the interference of four laser beams with a suitable arrangement of light polarizations [26]:

$$V(\mathbf{r}) \propto \sum_{m=1}^{3} \cos(\mathbf{K}_m \cdot \mathbf{r}) - \cos(\mathbf{K}_0 \cdot \mathbf{r}).$$

Here $\mathbf{K}_m = (\pi/2a)\, \hat{\mathbf{n}}_m$ is the laser wave vector, and a is the nearest-neighbor bond length. To obtain the orbital projectors on the nearest-neighbor bonds, we introduce a pseudovector $\boldsymbol{\mu} = (\mu^x, \mu^y, \mu^z) = (\lambda^{(6)}, \lambda^{(4)}, \lambda^{(1)})$ whose components are given by the three real-valued off-diagonal Gell-Mann matrices. The operators μ^a have the following nonzero elements: $\langle p_y | \mu^x | p_z \rangle = \langle p_z | \mu^y | p_x \rangle = \langle p_x | \mu^z | p_y \rangle = 1$. The orbital projectors along the four different bonds are

$$P^m = (I + \sqrt{3}\, \boldsymbol{\mu} \cdot \hat{\mathbf{n}}_m)/3, \quad (m = 0,1,2,3). \tag{6}$$

Substituting the above expression into Eq. (3) yields an effective Hamiltonian

$$H_{\text{diamond}} = \frac{2J}{3} \sum_{m=0}^{3} \sum_{\langle ij \rangle \| m} (\boldsymbol{\mu}_i \cdot \hat{\mathbf{n}}_m)(\boldsymbol{\mu}_j \cdot \hat{\mathbf{n}}_m). \tag{7}$$

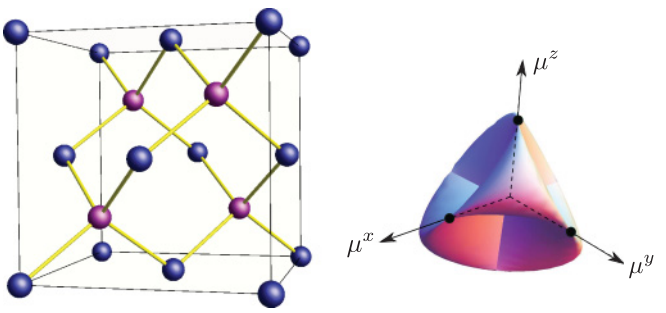

FIG. 3. (Color online) (a) Diamond optical lattice. (b) Domain of pseudovector $\langle \boldsymbol{\mu} \rangle$ for the diamond lattice.

Since the three matrices μ^a do not commute with each other, Eq. (7) defines a quantum "tetrahedral" Hamiltonian for pseudovectors $\boldsymbol{\mu}_i$ on the diamond lattice. The exchange interaction (7) is geometrically frustrated. To see this, consider a bond $\langle ij\rangle$ along the [111] direction. Its energy is minimized by orbital states $|\psi_i\rangle = |p_x + p_y + p_z\rangle/\sqrt{3}$ and $|\psi_j\rangle = |p_x - p_y\rangle/\sqrt{2}$. The corresponding expectation values of the pseudovector are $\langle\boldsymbol{\mu}_i\rangle = 2\,\hat{\mathbf{n}}_0/\sqrt{3}$ and $\langle\boldsymbol{\mu}_j\rangle = -\hat{\mathbf{z}}$, respectively. However, such an antiferro-orbital alignment cannot be achieved simultaneously on the other three $\langle 111\rangle$ bonds attached to site i.

To understand the ground-state structure, we first minimize the Hamiltonian using the Gutzwiller ansatz

$$|\Psi\rangle = \prod_i |\psi_i\rangle = \prod_i |\theta_i,\phi_i\rangle. \tag{8}$$

The Gutzwiller wave function is a direct product of single-site orbitals, The orbital wave function at a given site is parametrized by two angles θ and ϕ:

$$|\psi\rangle = \sin\theta\cos\phi|p_x\rangle + \sin\theta\sin\phi|p_y\rangle + \cos\theta|p_z\rangle.$$

The expectation value of the pseudovector is

$$\langle\boldsymbol{\mu}\rangle = (\sin 2\theta\sin\phi, \sin 2\theta\cos\phi, \sin^2\theta\sin 2\phi). \tag{9}$$

Figure 3(b) shows the domain of $\langle\boldsymbol{\mu}\rangle$ which has a tetrahedral symmetry. We employ Monte Carlo simulations to minimize the resulting mean-field energy $E\{\langle\boldsymbol{\mu}_i\rangle\} = \langle\Psi|H_{\text{diamond}}|\Psi\rangle$, which is a function of the pseudovectors. Specifically, small changes of θ_i and ϕ_i are generated randomly and Eq. (9) is used to compute the change in $\langle\boldsymbol{\mu}_i\rangle$ and the corresponding ΔE. These updates are then accepted according to detailed balancing. The Monte Carlo minimization yields many degenerate Gutzwiller ground states. We find that the pseudovectors in the ground states point along one of the six cubic directions, i.e., $\langle\boldsymbol{\mu}_i\rangle = \pm\hat{\mathbf{x}}$, $\pm\hat{\mathbf{y}}$, or $\pm\hat{\mathbf{z}}$ for all sites [Fig. 4], reminiscent of the six-vertex model. The corresponding orbital wave functions are $|\pm\hat{\mathbf{x}}\rangle = |p_y \pm p_z\rangle/\sqrt{2}$, and so on. The energy of each bond is exactly $\epsilon = -2J/9$ in the ground state.

Remarkably, the Gutzwiller ground states are also exact eigenstates of the Hamiltonian (7). To see this, we define an Ising variable for each of the nearest-neighbor bonds m attached to site i:

$$\sigma_i^m = \sqrt{3}\,\langle\boldsymbol{\mu}_i\rangle\cdot\hat{\mathbf{n}}_m = \pm 1, \quad (m = 0,1,2,3). \tag{10}$$

They satisfy the orbital ice rules

$$\sigma_i^m\,\sigma_j^m = -1 \tag{11}$$

for all nearest neighbors $\langle ij\rangle$ in the ground state. Now consider a given site i: if the Ising variable $\sigma_i^m = -1$ on the mth bond, then $|\psi_i\rangle$ is an eigenstate of the operator $\boldsymbol{\mu}_i\cdot\hat{\mathbf{n}}_m$ with eigenvalue $-1/\sqrt{3}$. On the other hand, for bonds with $\sigma_i^m = +1$, an extra term is generated when acted by the same operator. Specifically, let $|\psi_i\rangle = |+\hat{\mathbf{x}}\rangle$. The Ising variable is positive on [111] and $[1\bar{1}\bar{1}]$ bonds; we have

$$(\boldsymbol{\mu}_i\cdot\hat{\mathbf{n}}_m)\,|\psi_i\rangle = \pm\sqrt{2/3}\,|p_x\rangle + \sqrt{1/3}\,|\psi_i\rangle,$$

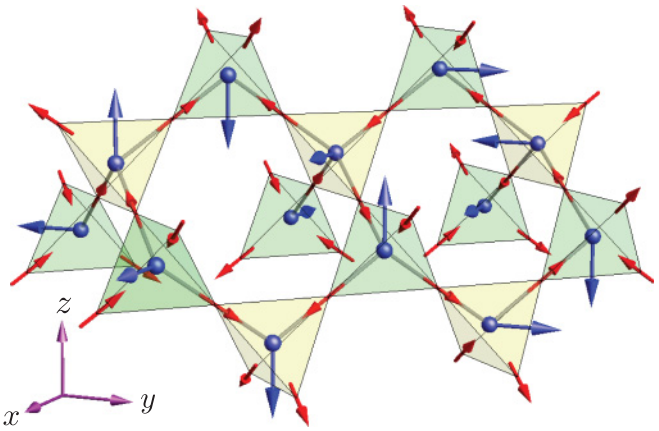

FIG. 4. (Color online) A configuration of the pseudovectors on the diamond lattice and its mapping to the spin-ice state on the medial pyrochlore lattice. The pseudovector only assumes six different values $\langle\boldsymbol{\mu}_i\rangle = \pm\hat{\mathbf{x}}$, $\pm\hat{\mathbf{y}}$, and $\pm\hat{\mathbf{z}}$ in the ground states, corresponding to $(p_y \pm p_z)$, $(p_z \pm p_x)$, and $(p_x \pm p_y)$ orbitals, respectively. These six orbital configurations are mapped to the six 2-in-2-out ice states on a tetrahedron Eq. (12).

with $\pm$ sign corresponding to $m = 0$ and 1, respectively. Applying the combined bond operator on the Gutzwiller wave function yields

$$(\boldsymbol{\mu}_i\cdot\hat{\mathbf{n}}_m)(\boldsymbol{\mu}_j\cdot\hat{\mathbf{n}}_m)|\Psi\rangle = \mp\sqrt{2}/3\,|p_x\rangle_i\otimes|\tilde{\Psi}_i\rangle - 1/3\,|\Psi\rangle,$$

where $|\tilde{\Psi}_i\rangle \equiv \prod_{k\neq i}|\psi_k\rangle$. Note that the nearest-neighbor site $j = j(m)$ depends on the bond index m. The two extra terms with opposite signs cancel each other when summed over $m = 0$ and 1. The Gutzwiller state $|\Psi\rangle$ is thus an eigenstate of the sum of the two bond operators with positive σ_i^m. Similar results hold for $|\psi_i\rangle = |\pm\hat{\mathbf{y}}\rangle$ or $|\pm\hat{\mathbf{z}}\rangle$. Since each site has two bonds with $\sigma_i^m = +1$ attached to it, the extra terms cancel out when summed over all bonds. Consequently, the Gutzwiller state $|\Psi\rangle$ is an exact eigenstate of the full Hamiltonian. We also performed exact diagonalization of Eq. (7) on a finite system of eight sites. With periodic boundary conditions, we find a huge degeneracy of the ground states which are indeed described by the Gutzwiller product. We now employ the fact that pyrochlore is the *medial* lattice of a diamond to examine the degeneracy and structure of the quantum ground states. As shown in Fig. 4, a pyrochlore magnet can be constructed by placing spins at the bond midpoints of a diamond lattice. This construction allows us to map the pseudovector field $\langle\boldsymbol{\mu}_i\rangle$ to a spin-ice state on the pyrochlore lattice. Specifically, we label spins on a pyrochlore lattice by bond index $\langle ij\rangle$ of the diamond lattice and use the Ising variables (10) to define its direction:

$$\mathbf{S}_{\langle ij\rangle} = +\sigma_i^m\,\hat{\mathbf{n}}_m = -\sigma_j^m\,\hat{\mathbf{n}}_m. \tag{12}$$

Here $\hat{\mathbf{n}}_m$ is a unit vector pointing from sites i to j. Note that the diamond-lattice sites are located at centers of tetrahedra in the pyrochlore lattice; the above mapping shows that the six distinct values of pseudovectors in the ground state, i.e., $\langle\boldsymbol{\mu}_i\rangle = \pm\hat{\mathbf{x}}$, $\pm\hat{\mathbf{y}}$, and $\pm\hat{\mathbf{z}}$, correspond to the six different 2-in-2-out ice states on a tetrahedron as demonstrated in Fig. 4. The ground-state degeneracy of the diamond orbital model can thus be calculated using the so-called Pauling estimate which gives a residual entropy per site $s_0 \approx k_B \ln 3/2 \approx 0.405\,k_B$.

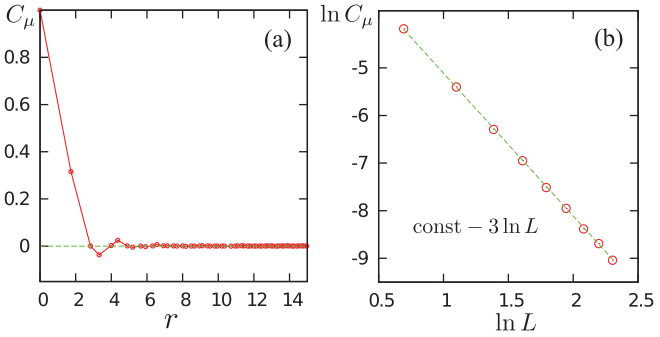

FIG. 5. (Color online) (a) Orbital correlation function $C_\mu(r) = \langle \boldsymbol{\mu}(r) \cdot \boldsymbol{\mu}(0) \rangle$ as a function of distance r in the quantum ground state of Hamiltonian (7). (b) $\ln C_\mu(L/2)$ as a function of $\ln L$; here $C_\mu(L/2)$ is the correlation function between sites separated by half the linear size L along a $\langle 110 \rangle$ chain of the lattice. The linear dependence in the log-log plot indicates a power-law decay: $C_\mu(L/2) \sim L^{-3}$.

The above mapping also makes it possible to compute orbital correlation functions by performing classical Monte Carlo simulations on pyrochlore spin ice. Since single-spin flip violates the ice rules, here we use the nonlocal loop moves to navigate the manifold of spin-ice ground states [27,28]; the results are shown in Fig. 5. The correlation function $C_\mu(r) = \langle \boldsymbol{\mu}(r) \cdot \boldsymbol{\mu}(0) \rangle$ decays rather rapidly with the separation of spins. It is interesting to note that the pseudovector is related to the divergence-free flux via $\mathbf{B}(\mathbf{r}_i) \sim \pm \langle \boldsymbol{\mu}_i \rangle$, where the $\pm$ sign refers to the two sublattices of the diamond lattice. As discussed in the Introduction, the magnetic field $\mathbf{B}$, hence the pseudovectors, displays a dipolar-like correlation function at long distances, as confirmed by our Monte Carlo simulations [Fig. 5(b)].

V. SUMMARY AND DISCUSSION

To summarize, we have investigated the orbital exchange physics of p-band spinless fermions on both cubic and diamond lattices. In both cases we have found a macroscopic ground-state degeneracy. The frustrated orbital interaction on the cubic lattice is governed by a classical three-state anisotropic Potts model. The ground state retains a finite entropy density $s_0 \approx 0.599 k_B$ per site. The orbital correlation function decays exponentially at large distances. We have also derived a quantum tetrahedral model describing orbital interactions on the diamond lattice. We have obtained exact quantum many-body ground states which are extensively degenerate with a residual entropy density $s_0 \approx k_B \ln 3/2 \approx 0.405 k_B$. By mapping the degenerate quantum ground states to spin-ice states on a pyrochlore lattice, we have shown that the fermionic p-band Mott insulators on a diamond lattice can be viewed as an orbital analog of the frustrated ice phase I_c of water.

The huge degeneracy of orbital ice also helps circumvent the entropy obstacle in its experimental realization. As noted in Ref. [29], a major challenge in creating strongly correlated phases in cold-atom systems is reaching the low level of entropies in such states. In this respect, the macroscopic residual entropy of the orbital ice renders the Coulomb phase much easier to realize in cold-atom optical lattices.

It is worth noting that the orbital ice model presented in this paper is different in nature from most conventional ice systems. First, the fundamental degrees of freedom of orbital ice are orbital triplets defined on the diamond lattice, whereas those of the conventional ice models are Ising-like variables on pyrochlore. Second, the pyrochlore ice models with the ice rules explicitly incorporated into the Hamiltonian are essentially classical systems. On the other hand, the orbital ice is an intrinsic quantum model. The orbital ice rules are emergent phenomena resulting from the orbital exchange dynamics. This is a rare example of emergent geometrical frustration in three dimensions. As usually happens in highly frustrated systems, the huge orbital degeneracy renders the ice phase susceptible to nominally small perturbations. Various interesting phases could emerge from the orbital Coulomb phase. Finally, it is also of great interest to examine the elementary excitations of the orbital ice model.

ACKNOWLEDGMENTS

G.W.C. thanks insightful discussions with C. D. Batista and the support of ICAM and NSF Grant DMR-0844115. C.W. acknowledges the support of NSF under DMR-1105945 and AFOSR-YIP program.

[1] V. F. Petrenko and R. W. Whitworth, *Physics of Ice* (Oxford, New York, 1999).
[2] For a review on spin ice, see S. T. Bramwell and M. J. P. Gingras, Science **294**, 1495 (2001), and references therein.
[3] A. P. Ramirez, A. Hayashi, R. J. Cava, R. B. Siddharthan, and S. Shastry, Nature (London) **399**, 333 (1999).
[4] C. Castelnovo, R. Moessner, and S. L. Sondhi, Nature (London) **451**, 42 (2008).
[5] R. F. Wang *et al.*, Nature (London) **439**, 303 (2006).
[6] M. Tanaka, E. Saitoh, H. Miyajima, T. Yamaoka, and Y. Iye, Phys. Rev. B **73**, 052411 (2006).
[7] A. Libál, C. Reichhardt, and C. J. Olson Reichhardt, Phys. Rev. Lett. **97**, 228302 (2006).
[8] A. Libál, C. J. Olson Reichhardt, and C. Reichhardt, Phys. Rev. Lett. **102**, 237004 (2009).
[9] Z. Nussinov, C. D. Batista, B. Normand, and S. A. Trugman, Phys. Rev. B **75**, 094411 (2007).
[10] C. L. Henley, Annu. Rev. Condens. Matter Phys. **1**, 179 (2010).
[11] M. Lewenstein *et al.*, Adv. Phys. **56**, 243 (2007).
[12] I. Bloch, J. Dalibard, and W. Zwerge, Rev. Mod. Phys. **80**, 885 (2008).
[13] M. Lewenstein and W. V. Liu, Nat. Phys. **7**, 101 (2011).
[14] C. Wu, Phys. Rev. Lett. **100**, 200406 (2008); the cubic optical lattice has been briefly discussed in C. Wu, e-print arXiv:0801.0888v1.
[15] E. Zhao and W. V. Liu, Phys. Rev. Lett. **100**, 160403 (2008).

[16] A. Nagano, M. Naka, J. Nasu, and S. Ishihara, Phys. Rev. Lett. **99**, 217202 (2007).
[17] D. I. Khomskii and M. V. Mostovoy, J. Phys. A **36**, 9197 (2003).
[18] G.-W. Chern, N. Perkins, and Z. Hao, Phys. Rev. B **81**, 125127 (2010).
[19] A. Isacsson and S. M. Girvin, Phys. Rev. A **72**, 053604 (2005).
[20] K. Goyal, I. Reichenbach, and I. Deutsch, Phys. Rev. A **82**, 062704 (2010).
[21] S. Blatt, T. L. Nicholson, B. J. Bloom, J. R. Williams, J. W. Thomsen, P. S. Julienne, and J. Ye, Phys. Rev. Lett. **107**, 073202 (2011).
[22] P. Hauke *et al.*, Phys. Rev. A **84**, 051603 (2011).
[23] Z. Nussinov *et al.*, Europhys. Lett. **67**, 990 (2004).
[24] A. van Rynbach, S. Todo, and S. Trebst, Phys. Rev. Lett. **105**, 146402 (2010).
[25] S. Wenzel and A. Läuchli, Phys. Rev. Lett. **106**, 197201 (2011).
[26] O. Toader, T. Y. M. Chan, and S. John, Phys. Rev. Lett. **92**, 043905 (2004).
[27] G. T. Barkema and M. E. J. Newman, Phys. Rev. E **57**, 1155 (1998).
[28] R. G. Melko and M. J. P. Gingras, J. Phys. Condens. Matter **16**, R1277 (2004).
[29] T.-L. Ho and Qi Zhou, Proc. Natl. Acad. Sci. USA **106**, 6916 (2009).